DALTON
FULL PAPER

Solid-state NMR studies of fluorinated diazadiphosphetidines

Robin K. Harris * and Lindsey A. Crowe

University of Durham, Department of Chemistry, South Road, Durham, UK DH1 3LE.
E-mail: r.k.harris@dur.ac.uk

Received 3rd September 1999, Accepted 25th October 1999

A solid-state NMR study of three diazadiphosphetidines with fluorine substituents has been carried out in order to obtain information on structural and dynamic properties. The ^{19}F and ^{31}P spectra are discussed in relation to X-ray results. The NMR data depend on the substituents at both the phosphorus and nitrogen positions, and motional properties observed in solution-state NMR are slowed in the solid state, but can still be investigated. Axial and equatorial fluorine positions have been distinguished by (fluorine) chemical shift, effective shielding anisotropies and isotropic (J_{PF}) coupling for $(PhF_2PNMe)_2$ at ambient probe temperature. Axial ↔ equatorial exchange is also shown to be slowed on the NMR timescale for $(F_3PNPh)_2$ at low temperature. Analysis of spinning sideband manifolds has yielded data on effective shielding anisotropies for both ^{31}P and ^{19}F spectra. Triple resonance ^{31}P-{^{19}F, ^{1}H} experiments have allowed the determination of true shielding tensor parameters. For $(Ph_2FPNMe)_2$ a triple-fit procedure has provided additional data, though not to high accuracy. Static ^{19}F and ^{31}P spectra, MAS ^{13}C and ^{15}N spectra and some relaxation times are also reported and discussed.

Introduction

Phosphorus pentafluoride and its organic derivatives with N-substituted hexamethyldisilanes give cyclic fluorophosphoranes (diazadiphosphetidines), which have received substantial attention. To produce substituted compounds, for example, *tert*-butyllithium will replace one F of a fully fluorinated compound with ^{t}Bu.[1] The synthesis route has been published previously[2] as has that for unsymmetrical diazadiphosphetidines.[3]

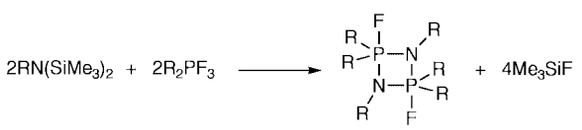

Electron-impact,[4] electron diffraction[5] and X-ray diffraction studies have been carried out on several of these compounds and similar systems. For example full crystal structures have been reported for $(Ph_2FPNMe)_2$,[6] $(PhF_2PNMe)_2$ and other fluorinated diazadiphosphetidines.[7] The compounds studied in the present investigation are of the form $(X_nY_{3-n}PNR)_2$, where R and X = alkyl or aryl and Y = F. Geometry and intramolecular motion have been the subjects of particular interest. NMR parameters (derived from solution-state studies) have been shown[2,6,8,9] to depend heavily on the nature of substituents and rates of intramolecular motion.

The dimeric structures consist of five-co-ordinate phosphorus within a four-membered ring. As one axial position and one equatorial position are occupied by the nitrogens in the ring, the remaining substituents on a given phosphorus can only occupy the trigonal bipyramidal positions still available. In the symmetrical fluorinated compounds one fluorine on each phosphorus will preferentially go axial, any other groups being forced into equatorial positions. These locations can generally be distinguished by (fluorine) chemical shifts and isotropic (J_{PF}) coupling constants. The magnitude of $J_{PF(axial)}$ is generally smaller than that of $J_{PF(equatorial)}$, and axial fluorines are deshielded relative to equatorial fluorines because axial bonds have less s character than equatorial. The trends in magnitudes of J_{PF} and δ_F can be illustrated by the following values from the literature: $(Et_2N)_2PF_3$ $|J_{PF(ax)}|$ 750, $|J_{PF(eq)}|$ 875;[10] Et_2NPEtF_3 $|J_{PF(ax)}|$ 830, $|J_{PF(eq)}|$ 984;[10] $MePF_3NMe_2$ $|J_{PF(ax)}|$ 803, $|J_{PF(eq)}|$ 964 Hz, $\delta_{F(ax)}$ −27.6, $\delta_{F(eq)}$ −69.0.[11]

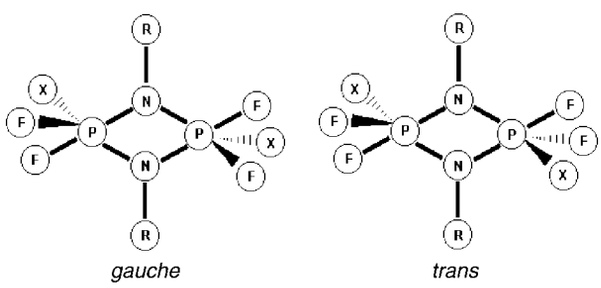

Fig. 1 The *trans*/*gauche* isomerism of disubstituted diazadiphosphetidines.

Isotropic scalar coupling constants, $^{1}J_{PF}$, are known to be negative.[12] When there are two fluorines on each phosphorus there is the possibility of *trans*/*gauche* isomerism across the planar ring (Fig. 1).[7,8] Values of $^{1}J_{PF}$ in the range −807 to −928 Hz were reported for *trans* and *gauche* isomers of a series of PF_2 diazadiphosphetidines, the *trans* isomers having values at the lower end of this range and the *gauche* isomer values generally having a magnitude over 900 Hz.[8] In such cases separate axial and equatorial values are not observed in solution-state studies, only an average $^{1}J_{PF}$. The crystal structure of $(PhF_2PNMe)_2$ shows it to be in the *trans* form,[8] whereas in solution *trans* ↔ *gauche* exchange is rapid on the NMR timescale above room temperature.

Despite the bonding around the PN ring tethering two co-ordination sites of each trigonal bipyramidal phosphorus, it has been found[8,9] that a form of motion can occur involving the other ligands. This is related to Berry pseudo-rotation.[13] The mechanism for this process can be thought of as follows. On transforming from one conformation to another the molecule will pass through an intermediate with a phosphorus centre of approximately tetragonal pyramidal geometry as the three non-bridging groups on phosphorus (axial and equatorial ligands) exchange through 120° about the plane of the four-membered ring.[8,9] The energy barrier for this process depends on the substituents on phosphorus, which will restrict such a process, and also on the rest of the molecule (the substituents on nitrogen), as will be shown for solid compounds in the variable temperature work described below. Careful choice of R and X groups must be made to observe this exchange process on the NMR timescale. If the groups are small, motion will be rapid and an

average will be seen at room temperature. If R and X are very large, motion will be slowed and, on the NMR timescale, the spectrum representing the rigid molecule will be observed at ambient probe temperatures. The ideal case will have a coalescence temperature for the motion within the accessible temperature range of the probe specifications. Harris and co-workers[9,14] have described pseudo-rotation processes in the solution state for diazadiphosphetidines involving the possible pseudo-rotamers in several similar compounds: axial–equatorial fluorine exchange, *gauche–trans* exchange and P–N bond equilibration.

All previous NMR studies on these, and closely similar, systems have been made in the solution state.[14] The aim of this work was to see how crystal packing and other solid-state effects influence the structure and symmetry of the systems, and also to test whether pseudo-rotation effects can be observed by NMR in the solid state, and, if so, over what temperature range. In general, solution-state data have been used for comparison with newly acquired solid-state data for confirmation of shifts and couplings, and also to distinguish any motional differences. These solution-state values are, in general, averages, where for rigid solids one can expect to distinguish axial and equatorial arrangements and to obtain information on anisotropic interactions. It proved possible, in the present study, to gain control over the rate of motion both by varying the experimental temperature and by controlling the substituents.

Magic-angle spinning is normally essential for obtaining high-resolution spectra for solids. In the cases of proton and fluorine solid-state NMR, homonuclear interactions have sometimes necessitated the use of multiple-pulse sequences[15,16] or high-speed spinning[17] to produce acceptable resolution. In order to produce high-resolution fluorine spectra the addition of proton decoupling is often necessary. High-power proton decoupling is applied as in other heteronuclear cases, but problems can arise as there is only 6% difference between the proton and fluorine resonance frequencies.[18,19] This will cause the effect known as the Bloch–Siegert shift, which will result in an apparent change in the chemical shifts of the fluorines on application of proton decoupling.[20] At 200 MHz this is a shift of around 2 ppm and has been taken account of by running the reference C_6F_6 sample with the proton frequency on. Owing to the close proximity of the frequencies, a custom-built two-channel probe is required. Isolation between the two channels is essential, and this is incorporated into the HF probe design. It is also necessary to use specific narrow-pass filters in the rf lines, to give improved separation of frequencies. Spectra recorded observing other nuclei, such as phosphorus, require high-power proton decoupling and are often simplified by additional decoupling, *e.g.* of fluorine.[21,22]

Although spinning sidebands are sometimes removed from solid-state spectra for simplicity, in many cases (such as coupled systems) a careful choice of spinning speed can lead to extraction of additional information (when no overlap of resonances occurs). In favourable cases the sideband manifolds in coupled systems can be simulated to obtain shielding anisotropy, shielding asymmetry and D' (a term which includes both D, the dipolar interaction, which can be calculated from a known internuclear distance, and the anisotropic indirect coupling ΔJ). For example, in the simplest case of an isolated two-spin system such as a PF doublet, the two spinning sideband manifolds in either ^{19}F or ^{31}P will differ from each other, with one stretched and the other compressed. This effect has been described previously for both the PC and PF cases.[23,24] An observable scalar (isotropic) splitting is essential to distinguish the two manifolds.

Throughout this article we use a definition of tensor components in which, for instance, $|\sigma_{33} - \sigma_{iso}| \geq |\sigma_{11} - \sigma_{iso}| \geq |\sigma_{22} - \sigma_{iso}|$, with anisotropy $\zeta = \sigma_{33} - \sigma_{iso}$. The effective anisotropy, ζ_{eff}, for a given spinning sideband manifold can be found in terms of eqn. (1), which assumes co-axiality of the true shielding

$$\zeta_{eff} = \zeta - (2\Sigma m_x D'/\nu_0) \quad (1)$$

anisotropy (ζ) and D', where $m_x = \pm\frac{1}{2}$ (the spin component quantum number for the relevant heteronucleus), $D' = D - (\Delta J/3)$ is the observed pseudo-dipolar interaction, and ν_0 is the precession frequency. It is assumed that the J and D tensors are co-axial, and asymmetry in J is ignored; D is defined in frequency units by eqn. (2) (where μ_o is the permeability constant

$$D = \frac{\mu_o}{4\pi}\gamma_P\gamma_F\frac{\hbar}{2\pi}r_{PF}^{-3} \quad (2)$$

and the γ values are magnetogyric ratios) and may readily be calculated if r_{PF} is known from diffraction experiments. Detailed equations for the effective tensor components in cases where ζ and D' are not coaxial have been given.[23,25] These can be used to derive the Euler angles linking $\boldsymbol{\sigma}$ and $\boldsymbol{D'}$ as well as the values of the tensor components, but only if experimental information is available over and above (for a two-spin case) the two spinning sideband manifolds from a coupled spectrum. In the cases considered here it is in principle possible simultaneously to fit[26,27] two spinning sideband manifolds from coupled spectra together with one manifold from a decoupled spectrum (at least for ^{31}P spectra). However, to derive all five parameters requires very high quality spectra, which were difficult to obtain in the present investigation. Moreover no triple-fit procedure can be carried out for ^{19}F work, since probe limitations mean phosphorus-decoupled fluorine spectra can only be recorded without proton decoupling, and hence good quality spectra cannot be obtained.

In the work reported here a series of diazadiphosphetidines has been investigated to determine their structural and dynamic properties in the solid state. The number of fluorines and the nature of the other substituents have been altered to investigate rates of motion, symmetry and coupling patterns (references for solution-state NMR and crystal structures are: $(Ph_2FPNMe)_2$,[6] $(PhF_2PNMe)_2$,[7,8,28] $(F_3PNMe)_2$[9]). Solid-state NMR spectra have been recorded for ^{31}P, ^{19}F, ^{13}C, and ^{15}N with various decoupling and cross-polarisation combinations. The first two nuclei listed are particularly useful because of their high sensitivity and 100% natural abundance, and because the strong interactions between them give two routes to complementary information. Study of the remaining nuclei in a molecule helps to complete the structural information.

Results and discussion

General features of ^{19}F and ^{31}P NMR spectra

Isotropic chemical shifts were established by variable spin-rate experiments. In all systems containing one or more fluorine atoms bonded to each phosphorus the splittings arising from the directly bonded (P, F) coupling constant, $^1J_{PF}$, are clearly resolved. The identity and magnitude of these splittings were confirmed by comparison of coupled spectra from each nucleus, together with P{F,H} and F{P} spectra. Table 1 gives a summary of chemical shift data for all the compounds studied, including comparisons with solution-state results from the literature.

Several general observations can be illustrated by the simplest P–F case, $(Ph_2FPNMe)_2$. The phosphorus and fluorine spectra are shown in Figs. 2 and 3 respectively. It is clear that in each case only a single type of site exists for the relevant nucleus. The ^{15}N NMR spectrum also seems to contain a single isotropic peak (see below). Thus the crystallographic asymmetric unit contains a single PFN group. The published diffraction results[6] include both a monoclinic crystal (for the monomer) and a dimeric, triclinic crystal. In the latter case there are two non-equivalent but centrosymmetric molecules in the unit cell. However, significant differences in bond lengths

Table 1 Chemical shifts and coupling constants[a]

Compound	Chemical shift, δ			Observed ^{31}P $\lvert^1J_{PF}\rvert$[b]/Hz ± 20	Observed ^{19}F $\lvert^1J_{PF}\rvert$[b]/Hz ± 30
	^{31}P	^{19}F	^{13}C		
$(Ph_2FPNMe)_2$	−67.4	−25.6	31	700	700
	(−64.3)	(−23.6)	≈132	(689)	(689)
$(PhF_2PNMe)_2$	−55.3	−43.1 (ax)	27.8	890[d]	623 (ax),
(*trans*)	(−55.1)	−78.2 (eq)	128.4	(865[d])	1237 (eq)
		(−63.6)[c]	132.6		
$(F_3PNPh)_2$	−73.4	−74.2		890[g]	947
	(−71.5[e])	(−80.7[e])		(922[e])	(922[e])
		ca. −50[f]			
		ca. −90[f]			

[a] Solution-state data are given in parentheses (from refs. 6, 8 and 29). [b] For the solid state the value quoted is derived from the splitting between the most intense pair of lines and may therefore involve $^3J_{PF}$ as well. [c] Average for axial and equatorial fluorines. [d] This is the average, $\frac{1}{2}|^1J_{PF}(ax) + {}^1J_{PF}(eq)|$. [e] For $(F_3PNMe)_2$, from refs. 13 and 34. [f] Separate values for axial and equatorial fluorines, from low-temperature spectra. [g] Average value (from ambient temperature measurement; separate low temperature values cannot be resolved).

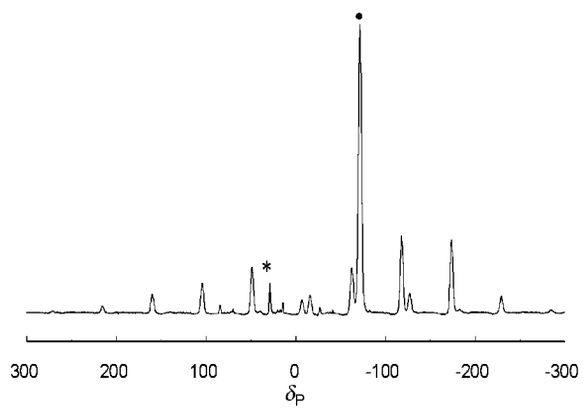

Fig. 2 Phosphorus-31 NMR spectrum of $(Ph_2FPNMe)_2$ at 81 MHz. Cross-polarisation from protons and high-power proton decoupling were employed. The isotropic doublet is marked ● and a phosphorus-containing impurity indicated by *. Contact time 5 ms, number of transients 36, spin rate 4.5 kHz, recycle delay 30 s.

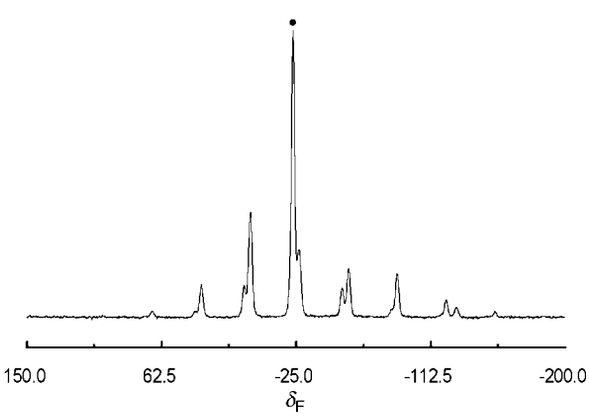

Fig. 3 Fluorine-19 NMR spectrum of $(Ph_2FPNMe)_2$ at 188 MHz. Cross-polarisation from protons and high-power proton decoupling were employed. The symbol ● marks the centreband doublet. Contact time 1 ms, number of transients 100, spin rate 6 kHz, recycle delay 30 s.

and angles are not observed between the two molecules and we do not see separate NMR signals from them. By acquisition of an X-ray powder diffraction pattern it is possible to conclude (from comparison with the powder pattern predicted from the published single-crystal results) that the sample used in this work is definitely the triclinic (dimeric) structure. In both ^{19}F and ^{31}P spectra there is an observable splitting arising from $^1J_{PF}$. The spinning sideband manifolds are extensive in range. The isotropic shifts are measured as δ_P −67.4 and δ_F −25.6 for $(Ph_2FPNMe)_2$, close to those reported for solutions. The coupling constant $|^1J_{PF}|$ is 700 Hz (within experimental error of the

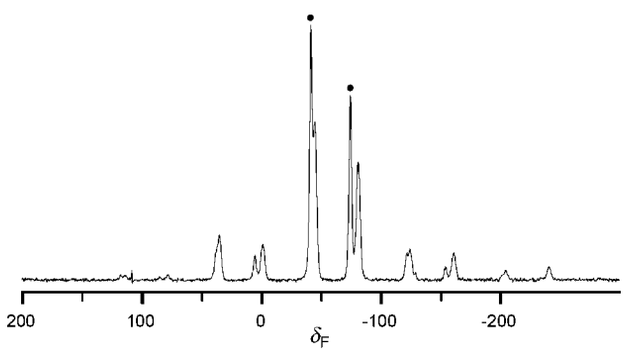

Fig. 4 The ^{19}F-{^{1}H} NMR spectrum of $(PhF_2PNMe)_2$ with cross-polarisation from protons. Centrebands marked ● represent axial (high frequency) and equatorial (low frequency) fluorine signals. Contact time 5 ms, number of transients 64, spin rate 15 kHz, recycle delay 60 s.

solution-state value). The value of δ_F is consistent with the expected position for a single axial fluorine attached to trigonal bipyramidal phosphorus due to substituent electronegativity considerations as well as by comparison with the solution-state value of δ −23.61.[6] The long-range (P, F) isotropic coupling constant is not large enough (being 5.8 Hz in magnitude in the solution state[6]) to be observed within the resolution of these MAS NMR spectra. However, because the spin system involved is symmetrical, the observed splitting, as with the other cases discussed in this article, may not be precisely $|^1J_{PF}|$ but may involve $|^3J_{PF}|$.[2,29] Moreover, complications can arise from other couplings in the system.[29] Values of $^2J_{PP}$ for diazadiphosphetidines are significant, being in the range 20–140 Hz in magnitude in most cases[1,30] (and as high as 210 Hz for $(F_3PNMe)_2$),[9] but it is not feasible to take such couplings into account. Further complexities occur in principle for spinning sideband shapes in MAS spectra arising from homonuclear dipolar coupling[31] but again these have necessarily been ignored given the linewidths observed, which are *ca.* 320 Hz for ^{31}P and *ca.* 480 Hz for ^{19}F. It may be noted that values for D_{PP} for diazadiphosphetidines are *ca.* 1 kHz and D_{FF} for the geminal fluorines in, for example, $(RF_2PNMe)_2$ is *ca.* 10 kHz. However, since no splittings are visible in the spectrum arising from $^2J_{PP}$ or $^2J_{FF}$, the effects of these dipolar interactions on spinning sideband intensities will be averaged away, very effectively for D_{PP} and for cross-ring D_{FF}, which are much less than ζ. This means the case of $(Ph_2FPNMe)_2$ is relatively straightforward, whereas complications arising from geminal D_{FF} may be significant for $(RF_2PNMe)_2$ and $(F_3PNPh)_2$.

When a second fluorine is introduced around the phosphorus there then exists the possibility of axial and equatorial differences. From the centreband peaks in the ^{19}F spectrum of $(PhF_2PNMe)_2$ it is clear that there are distinct axial and equatorial environments (Fig. 4), though the crystallographic

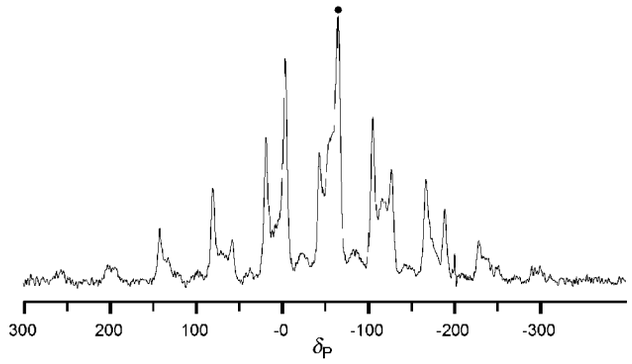

Fig. 5 The ^{31}P-{^{1}H} NMR spectrum of $(PhF_2PNMe)_2$ with cross-polarisation from protons, each band showing complex coupling patterns. The symbol • marks the centreband. Contact time 1 ms, number of transients 180, spin rate 5 kHz, recycle delay 60 s.

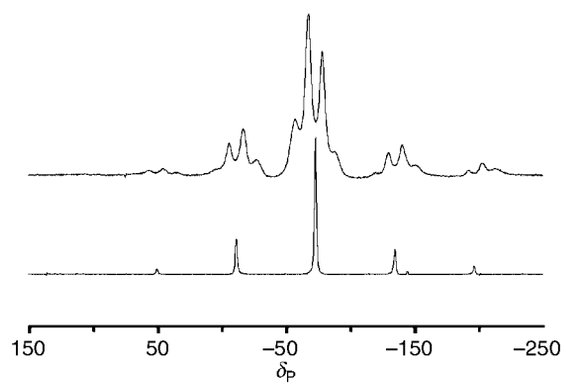

Fig. 6 Phosphorus-31 NMR spectrum of $(F_3PNPh)_2$ with CP from protons: upper spectrum {H}, lower spectrum {H,F}. Contact time 10 ms, number of transients 360, spin rate 5 kHz, recycle delay 30 s.

asymmetric unit evidently contains a single PF_2 group. This is the first time separate data for axial and equatorial fluorines have been obtained for a symmetrical diazadiphosphetidine. The solution-state chemical shift is approximately midway between the two values found for the solid, as expected. The crystal structure[7] describes a *trans* configuration with a crystallographic centre of symmetry, and the molecule contains a planar P_2N_2 ring. The NMR data are consistent with this crystal structure. The J_{PF} coupling constants differ markedly in magnitude (by approximately a factor of two), depending on the position of the fluorine (the s character of the bond changes between equatorial and axial sites in a trigonal bipyramid), as can be seen from both ^{31}P and ^{19}F spectra. No additional splittings arising from $^{2}J_{FF}$ could be resolved in the ^{19}F spectrum. For distinct fluorine sites to be observable the system must be towards the low temperature exchange limit, at least below coalescence. For temperatures at which the available energy is sufficient to overcome the pseudo-rotation barrier average values for both chemical shift and indirect coupling constant would be observed. The single phosphorus isotropic shift shows a complex pattern arising from different couplings to axial and equatorial fluorine nuclei.

For $(RF_2PNMe)_2$ the spectral pattern for each nucleus is influenced by the spin state of the other. The coupling patterns are particularly complex in the phosphorus region at the slow motion limit. The separation of the outer lines of the centreband is a sum of (P, F) coupling constants (see below). The mixing of states with the same Σm_F will cause the inner ^{31}P peaks, for example, to become unresolved. Both of these effects can be seen in the spectrum of $(PhF_2PNMe)_2$ (Fig. 5). To represent the mixing of states more clearly we will take the general case of a PF_2 dimer. In principle, the spin system is of the type $[ABX]_2$. There are four F atoms which can each exist in either α or β states, and the sum of these spin states will determine

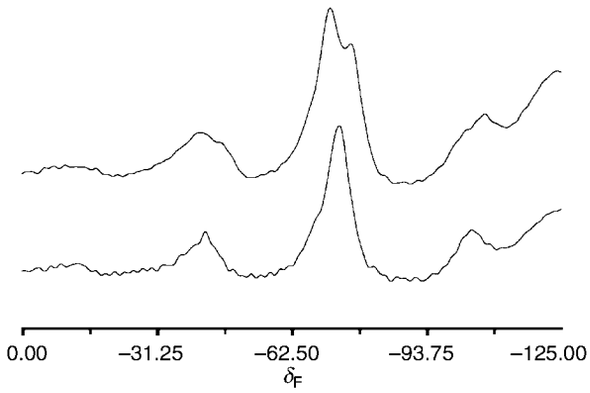

Fig. 7 Direct polarisation fluorine-19 NMR spectrum of $(F_3PNPh)_2$: upper spectrum (single resonance); lower spectrum {P} (to low frequency of −100 ppm, on the edge of the figure, is the broad probe background). Number of transients 200, spin rate 4.1 kHz, recycle delay 5 s.

whether the P transition is unique. With ααααα and βββββ the values of Σm_F are +2 and −2 respectively. No other combinations give these values and these states therefore give rise to the two intense outer ^{31}P transitions. There is no unique state representing $\Sigma m_F = -1, 0, +1$, and therefore transitions involving these will form the mixed, unresolved central portion of the band. The total splitting of the outer lines can be seen to be $|^{1}J_{PFa} + {}^{1}J_{PFb} + {}^{3}J_{PFa} + {}^{3}J_{PFb}|$. In practice $|^{3}J_{PF}| \ll |^{1}J_{PF}|$,[8] so the effect of cross-ring (P,F) coupling is likely to be small, as will be the more complicated effect of $^{2}J_{PP}$ and $^{2}J_{FF}$.

For $(F_3PNPh)_2$ we have obtained chemical shift values of δ_P −73.4 and δ_F −74.2. Our observations suggest that there is probably only one PF_3 group in the crystallographic asymmetric unit; $|^{1}J_{PF}|$ measured from the fluorine spectrum (doublet at ambient probe temperature) is 947 Hz and an average value extracted from the phosphorus quartet is 890 Hz. The difference here will result in considerable part from the accuracy of the splitting measurement for the fairly broad lines. Solution-state data for comparison[9,32] are only available for $(F_3PNMe)_2$. Figs. 6 and 7 illustrate the effects of decoupling for $(F_3PNPh)_2$. The first shows the collapse of the phosphorus quartet (1 : 3 : 3 : 1 intensities over the complete manifold) to a singlet on application of fluorine decoupling. The effects of varying the frequency and power of the decoupling rf can also be monitored. In the case of $(F_3PNPh)_2$ the fluorine decoupling is efficient over a range of ±5 kHz around the on-resonance fluorine frequency. Away from this the ^{31}P lines broaden, and at an offset of 40 kHz from the ideal frequency a distorted coupling pattern begins to be seen. The F{P} experiment is an unusual one for the HFX probe, which is not normally used for fluorine observation. The close proximity of the proton and fluorine frequencies does not allow one to be observed while the other is being decoupled (in contrast to the situation with the specific HF probe) so that in many cases the fluorine spectrum would be sufficiently broadened by proton interactions as to become featureless. However, in this case, we retain some resolution of $^{1}J_{PF}$ even in the absence of proton decoupling. Unfortunately there is also a significant fluorine background signal for this probe, but this does not interfere with the centreband region of the spectrum (which was already clearly identified in F{H} experiments).

Fluorine-19 and phosphorus-31 spinning sideband analysis

Spinning sideband analysis has been carried out for $(Ph_2FPNMe)_2$ to determine shielding anisotropies and shielding asymmetries for both ^{31}P and ^{19}F. The protocol used initially assumed collinearity of tensors. Use of just the two spinning sideband manifolds from the J_{PF} doublets is unable to deal fully with cases lacking collinearity since there are only six

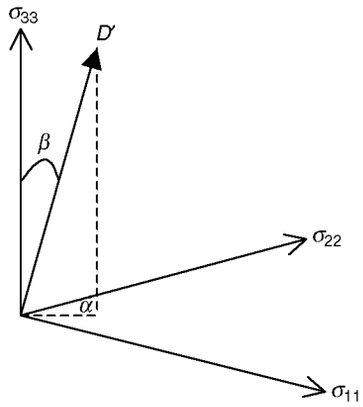

Fig. 8 Tensor orientation angles.

measurable effective tensor components but seven variables (three principal components of σ, D', $|J_{iso}|$ and two Euler angles relating D' to σ). However, ^{19}F decoupling gives a ^{31}P spinning sideband pattern that yields the principal components of σ immediately, so that the coupled spectrum can then be used to determine the remaining variables. In order to optimise the analysis we have fitted the ^{31}P-{^{19}F} decoupled spectrum and the two spinning sideband manifolds of the coupled spectrum simultaneously.[26,27] The computer program ssb97m, developed in house,[33] was used for this 'triple fit' analysis.

For the reported results, α and β are the polar angles defining the internuclear vector (*i.e.* the direction of the D' tensor axis) in the principal axis system of the shielding tensor. Thus, β is the angle between D' and σ_{33}, and α is the angle from σ_{22} of the projection of r_{PF} in the σ_{11}–σ_{22} plane. Fig. 8 can be used to illustrate the angles α and β quoted above. In fact, if β is 0°, α cannot be defined. However, the method used to calculate the angles means they are only accurate to within about 10° and therefore a value of zero simply indicates that the tensor lies close to the σ_{33} axis. Where the crystal structures are known, D can be calculated and a value for the anisotropy in J may be extracted if D' can be obtained.

Results for $(Ph_2FPNMe)_2$. For ^{31}P, effective anisotropies of the two separate spinning sideband manifolds are $\zeta_{eff} = -50$ and -265 ppm (with $\eta = 0.8$ and 0.3 respectively). The two values of ζ_{eff} show the stretching and compressing of the spinning sideband manifolds.[23] Analysis of the spinning sideband manifold of the decoupled spectrum shows that σ is asymmetric, indicating that collinearity of σ and D' is unlikely. A triple fit of the phosphorus spectra (two sideband manifolds for the coupled case and one for the ^{19}F-decoupled situation) gives $\zeta = -148$ ppm, $\eta = 0.4$, $D' = 10$ kHz and $\beta = 0°$ (within experimental error, leaving α essentially indeterminate). From D', the value of $\Delta J = -1.2$ kHz may be derived by using $r_{PF} = 1.686$ Å^6 ($D = 9.6$ kHz < D'). It should be noted that the difference between D and D' is fairly small compared to the expected uncertainty in D' (≈5 ppm was found for the values of effective anisotropy), meaning that the value of ΔJ derived is only an estimate. Significantly better quality data are required to obtain reasonable values of ΔJ, α and β. It may be noted that for two fluorophosphates Grimmer and co-workers[24,34] derived values of +2500 and +3660 Hz for ΔJ.

The sense of tensor distortions of the stretched and compressed subspectra described above shows[23,24] the relative signs of D' and J. The logic can be followed with the case of the PF spin pair in $(Ph_2FPNMe)_2$. From the static phosphorus spectrum with both proton and fluorine high-power decoupling, one can determine that the shielding anisotropy is negative (in agreement with the triple fit to the spinning sidebands). This is opposite to the two-spin case discussed in the literature,[23] and as σ_{33} is the least shielded component it will be the 'plus' subspectrum (relating to the $m_F = +\frac{1}{2}$ state) that is stretched. The

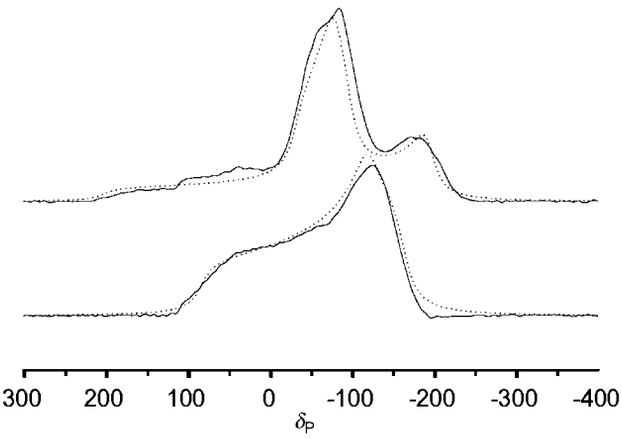

Fig. 9 Static phosphorus spectra of $(Ph_2FPNMe)_2$, using CP from ^{1}H: upper, P{H}; lower, P{H,F}. Solid lines, experimental spectra; dotted lines, simulated spectra. Contact time 5 ms, number of transients 360, recycle delay 30 s.

spinning sideband manifolds of the fluorine-coupled spectrum show that this state constitutes the high-frequency transition of the doublet caused by (P,F) scalar coupling. Thus, J_{PF} is found to be negative, in agreement with the known sign, obtained from solution-state spectra. As is obvious from Figs. 2 and 3, the ^{19}F case (which clearly has the low-frequency sideband manifold stretched) is the reverse of the ^{31}P situation, which immediately suggests the true ^{19}F shielding anisotropy is positive, as is in fact suggested by the single-fit analyses. The ^{31}P and ^{19}F effective tensor components from single fits for all three compounds, together with the results for ^{31}P-{^{19}F, ^{1}H} spectra, are given in Table 2.

For $(PhF_2PNMe)_2$ separate single fits of the fluorine-coupled phosphorus subspectra yield $\zeta_{eff} = -213$, 160 ppm and $\eta_{eff} = 0.9$, 0.4 for the outer lines. These calculations relate to the sum of the influences of the two fluorines, as explained above. Separate ^{19}F data sets are available for the axial and equatorial fluorines but the results may be significantly affected by the relatively large value of D_{FF}. The decoupled ^{31}P spectrum yields a value for the anisotropy of -156 ppm (≡ 12.6 kHz), which is similar to that for $(Ph_2FPNMe)_2$ and is of the same order as D_{PF}, thus explaining the significant intensity variations of the doublet components over the spinning sidebands. As for $(Ph_2FPNMe)_2$, the shielding tensor is asymmetric, underlining the fact that $\boldsymbol{\sigma}$ and $\boldsymbol{D}$ are not collinear. A ^{31}P triple fit is not feasible for $(PhF_2PNMe)_2$ because the two dipolar tensors have different orientations, introducing more variables.

For $(F_3PNMe)_2$ effective anisotropies are given in Table 2, from the manifolds of both the ^{31}P and ^{19}F spectra. These results differ significantly from those of the other two compounds but cannot be analysed more fully. However, it would appear to be likely that the ^{31}P and ^{19}F shielding anisotropies are both smaller in magnitude than for the other two compounds.

Static ^{19}F and ^{31}P spectra

Static phosphorus spectra have been recorded (Fig. 9). Use of a Hahn echo sequence (with interpulse delay time 20 μs) produces an acceptable lineshape as it results in accurate recording of the start of the fast-decaying broad signals. For $(Ph_2FPNMe)_2$ the ^{31}P-{^{1}H} spectrum shows the effects of ^{31}P,^{19}F dipolar coupling, with the overall shape consisting of two overlapping static subspectra. An impurity present in this sample was reduced in quantity by recrystallisation from toluene, but its signals are still visible, with isotropic shifts around 19 and 30 ppm. A single band is obtained when fluorine decoupling is applied (in addition to proton decoupling). Tensor results from static spectra are compared to those from spinning sideband analysis in Table 3. Comparison of the turning points for the coupled

Table 2 Tensor information from spinning sideband analysis

Compound	ζ_{eff} (η_{eff}) [$\sigma_{11} - \sigma_{iso}$, $\sigma_{22} - \sigma_{iso}$, $\sigma_{33} - \sigma_{iso}$][a]		
	Single fit of multiplet sidebands[b]		Single fit of decoupled spectra[c]
	^{31}P	^{19}F	^{31}P
$(Ph_2FPNMe)_2$	−265 (0.3) [231, 158, −202] −50 (0.8) [117, 77, 22]	−33 (0.8) [54, 26, −10] +108 (0.5) [−54, 2, 135]	−158 (0.7) [158, 143, −88]
$(PhF_2PNMe)_2$	−213 (0.9) [251, 50, −169] +160 (0.4) [−44, 16, 227]	+97 (0) [−6, −6, 138] (ax) −120 (1) [163, 46, −74] +96 (0) [26, 26, 172] (eq) +139 (0.6) [−32, 56, 221]	−156 (0.4) [169, 96, −100]
$(F_3PNPh)_2$[d]	−50 (0) [82, 82, 7] +84 (0.7) [4, 55, 154] +120 (0.4) [−7, 44, 198] +163 (0.3) [−17, 31, 251]	−23 (0) [82, 82, 46] +34 (0.5) [49, 66, 110]	+100 (0.5) [−3, 49, 173]

[a] The data for ζ_{eff} and the (effective) shielding tensor components are given in ppm. Note that the definitions (see text) imply switching of the effective components σ_{11} and σ_{33} depending on the position of σ_{22}, leading to a change of sign in ζ_{eff}. The statistical errors are ±5 ppm in ζ_{eff} and ±0.1 in η_{eff}, but these are likely to be underestimates of the true errors. [b] Effective anisotropies and asymmetries. [c] True shielding anisotropies and asymmetries. [d] Data for ambient probe temperature (fast axial ↔ equatorial fluorine exchange).

Table 3 Values of ^{31}P anisotropy $\zeta_{eff} = \sigma_{33} - \sigma_{iso}$ (asymmetry, η_{eff}) for $(Ph_2FPNMe)_2$

	MAS coupled		MAS F decoupled[a]	Static coupled		Static, F decoupled[a]
ζ_{eff}	−265	−50	−158	−265	−36	−150
η	0.3	0.8	0.7	0	0.5	0.3

[a] True shielding anisotropy and asymmetry.

and decoupled spectra helps to link the components of the effective tensors. The simulated spectra are the best fits by eye to the observed spectra. Errors in the resulting parameters will therefore be larger than for the MAS experiments. The discrepancy between 0 and 100 ppm in the coupled spectrum results from the remaining low-intensity impurity. A line-broadening parameter of 800 Hz in the computation was needed to give a similar shape to the experimental results. This gives some idea of the magnitudes of broadening effects (*e.g.* dipolar interactions other than $^1D_{PF}$) for the compound. The corresponding fluorine spectrum for this compound clearly consists of multiple lineshapes. The quality is not sufficient to provide accurate data.

As discussed above, the fluorine MAS spectrum of $(PhF_2PNMe)_2$ consists of two doublets (for axial and equatorial environments). The static lineshape consists of four overlapping static bands, with a stretched and compressed anisotropy, from J_{PF}-split components, for each of the fluorines (axial and equatorial). Approximate fitting by eye suggests the four static lineshapes have effective shielding anisotropy values of 97, 160, 97 and −140, in reasonable agreement with the MAS results, though those of −140 and 160 are about 20 ppm larger in magnitude than their counterparts from fitting of the spinning sideband manifolds. It is important to note that the spinning sideband analyses include an iterative fitting procedure, unlike the simulation of the static lineshapes, for which the spinning results were used as an initial estimate.

Variable temperature spectra

Changes with temperature are clearly illustrated (Fig. 10) in the ^{31}P NMR spectra of $(F_3PNPh)_2$. At ambient probe temperature all fluorines are equivalent and, on summing intensities of the multiplet peaks over the spinning sidebands of the phosphorus spectrum, one obtains a quartet of the expected ratio from coupling to three fluorines. Fast reorientation of the fluorine sites means that only the average shift and coupling constant are observed, as in solution. The splitting, $|^1J_{PF}|$, is one third of the remaining doublet splitting observed at low temperature,

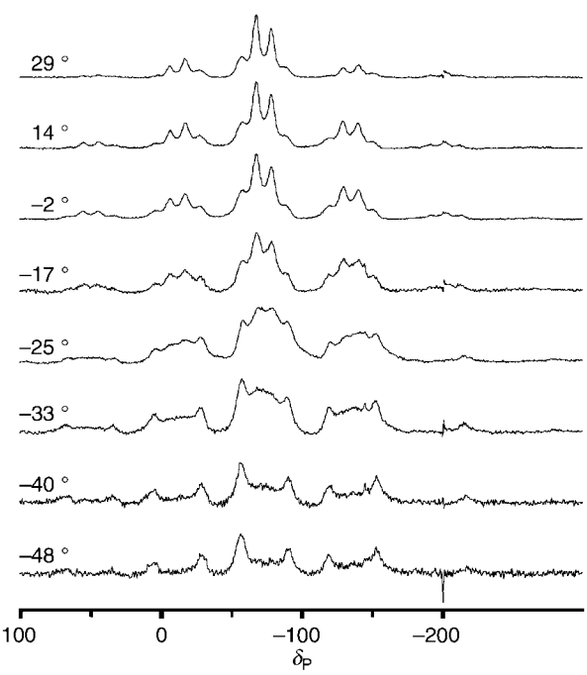

Fig. 10 Direct polarisation, proton-decoupled variable-temperature ^{31}P NMR spectra of $(F_3PNPh)_2$. Number of transients 128, spin rate 5 kHz, recycle delay 20 s.

when the fluorines have become inequivalent (Fig. 10). Owing to the slower pseudo-rotation at low temperature, the axial and equatorial fluorine sites will show their individual chemical shifts, and coupling constants will no longer be averaged. The ^{31}P spectrum will then be significantly more complex, resulting in broadening of the central two lines of the quartet. However, the outer quartet lines, arising from $\Sigma m_F = \pm 3/2$, are unaffected and remain relatively sharp at all temperatures. The corresponding variable-temperature fluorine spectra show the equivalence at room temperature, then a broadening and separation into two broad bands for axial and equatorial sites in a 1 : 2 intensity ratio at *ca.* −40 °C (Fig. 11). The resolved doublet at the lowest temperature, which does not change significantly with temperature, is that of an impurity. On an absolute scale it stays at constant intensity and shape, becoming more prominent as the diazadiphosphetidine peaks broaden. Lower temperatures would be required to see any narrowing of the separated bands and resolution of the coupling patterns. The coalescence temperature of the fluorine sites (*ca.* 40 °C) in $(F_3PNPh)_2$ provides an approximate estimate of the rate constant for the

Table 4 Motional effects relative to the NMR timescale

Compound	Motion at ambient temperature	Motion at low temperature (≈100 °C)
$(Ph_2FPNMe)_2$	—[a]	—[a]
$(PhF_2PNMe)_2$	Slow	Slow
$(F_3PNPh)_2$	Fast	Medium (two broad resonances)

[a] No information available since only a single ^{19}F site is observed.

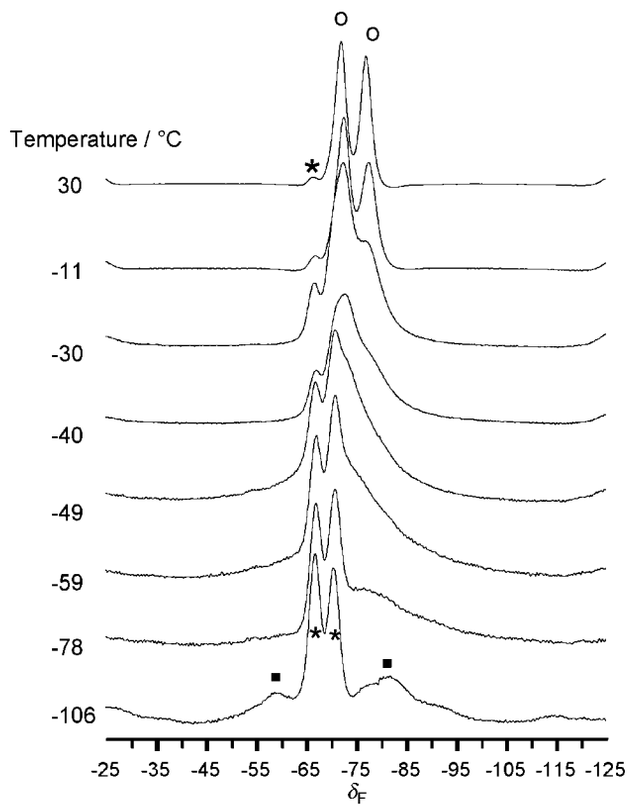

Fig. 11 Direct-polarisation ^{19}F-{^1H} NMR spectra of $(F_3PNPh)_2$ as a function of temperature. The vertical scales are plotted to equal maximum peak height. The doublet at δ −68 is a constant-intensity impurity. Number of transients 16, spin rate 10 kHz, recycle delay 60 s. High-temperature doublet O, low-temperature bands ■, impurity doublet (where visible) *.

axial ↔ equatorial process, namely 12000 s^{-1} from[35] $k = \pi\delta\nu/\sqrt{2}$. However, this assumes the low-temperature limit has been reached so that the chemical shift separation, $\delta\nu = 5400$ Hz, at the lowest temperature studied is the true value applicable for −40 °C (*i.e.* is temperature independent).

The variable-temperature experiments, and comparison of the different compounds at ambient temperature, show that different ranges of motion are accessed depending highly on the substituents. The fully fluorinated compound has less restriction to F exchange *via* pseudo-rotation, which is also the case for small R groups on nitrogen. However, for $(PhF_2PNMe)_2$ the motion is already sufficiently slow at room temperature to enable the separate fluorine environments to be seen. The barrier is lower for PF_3 compounds because of the symmetry involved in the pseudo-rotation process in such cases. Table 4 summarises the information as to which compounds exhibit observable motional effects relative to the NMR timescale over the temperature range ambient to −120 °C.

Nitrogen-15 NMR spectra

The ^{15}N spectra (Fig. 12) proved to be difficult to acquire, and it has only been possible to obtain data using the variable-amplitude cross-polarisation sequence (Ramp CP). The results

Table 5 ^{15}N chemical shifts and spectral parameters

Compound	Pulse sequence	Contact time/ms	Number of acquisitions	Line-width/ Hz	δ (^{15}N)
$(Ph_2FPNMe)_2$	CP	5	2000	66	−302
$(PhF_2PNMe)_2$	Ramp CP[a]	8	2000	200	−287
$(F_3PNPh)_2$	Ramp CP[a]	5	3300	80	−266

[a] 48 increments in proton CP power.

Table 6 Relaxation times

Compound	T_1^H[a]/s	T_1^F/s	$T_{1\rho}^H$/ms	T_{CP}/ms
$(Ph_2FPNMe)_2$	26	64	≈50[b] 68,[c] 20[c]	0.33[b]
$(PhF_2PNMe)_2$	24	156 (ax) 169 (eq)	*ca.* 700[d]	
$(F_3PNPh)_2$	2.5	0.3	Large	1.3[b]

[a] From $^1H \longrightarrow {}^{31}P$ CP following ^1H spin inversion. [b] From $^1H \longrightarrow {}^{31}P$ CP variable contact time experiment. These data are effective rather than true times (see text). [c] From proton-observe measurements. [d] From a variable contact time $^1H \longrightarrow {}^{19}F$ experiment (longest value only *ca.* 50 ms, so the result can only be considered as an estimate).

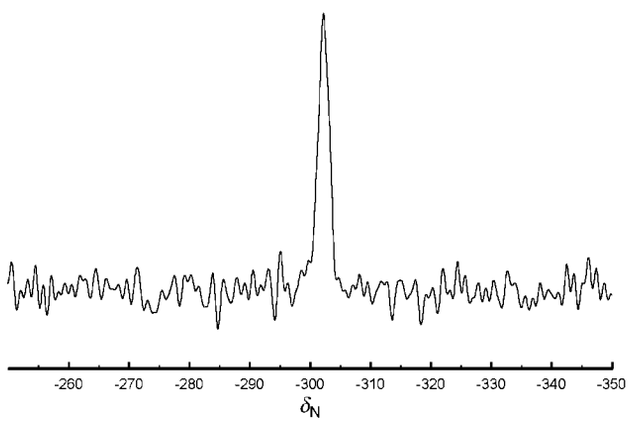

Fig. 12 Nitrogen-15 NMR spectrum of $(Ph_2FPNMe)_2$ at 30.4 MHz, using the Varian Unity Plus 300 spectrometer and CP from ^1H. Contact time 5 ms, number of transients 2000, spin rate 4.4 kHz, recycle delay 30 s.

and the spectral parameters used are summarised in Table 5. The single peaks observed in all cases suggest the asymmetric crystallographic units contain a single N, though that is known not to be the case for $(Ph_2FPNMe)_2$, see above. Nitrogen-15 chemical shifts observed over the series of fluorodiazadiphosphetidines show variations depending both on the nature of the adjacent R group attached to nitrogen and on the number of fluorine substituents at phosphorus, increase in the latter causing deshielding.

Relaxation times

The techniques used to measure relaxation times are given in the Experimental section. For T_1 measurements the ^{19}F spectrum was observed, with proton decoupling only during acquisition. Plots of the intensity characterised by the relaxation time included between 10 and 20 data points. The data are given in Table 6. The method of intensity measurement used to calculate the magnetisation curve will be a significant source of error in relaxation times. Depending on the observed spectrum, either peak height (if there is no overlap) or deconvolution to provide an integrated intensity is used. Intensities measured by both these methods are accurate to within about 2–8%, the

higher the noise level the greater the inaccuracy. In the present case there is a statistical uncertainty in T_1^H of about 8%. This will be the minimum error assuming stability of the spectrometer, negligible pulse imperfections and accurate representation of the lineshape over the whole experimental time. For $(Ph_2FPNMe)_2$, T_1^F is longer (64 s) than T_1^H (26 s), and hence cross-polarisation from protons gives a good signal in a shorter experiment time than direct polarisation. The value of T_1^F was therefore measured *via* $^1H \longrightarrow {}^{19}F$ CP, as described elsewhere,[36] with proton decoupling during acquisition. When abundant nuclei are being observed, the intensity curve with variable contact time may be a complex combination of parameters.[37] Observation of the spin-lock characteristics of the MAS proton spectrum directly should give true values for $T_{1\rho}^H$. The broad band is a combination of Me and Ph proton resonances and those for the latter decay much faster (have shorter $T_{1\rho}^H$) than those for the former. Deconvolution of the band into two broad resonances gave intensities fitting to values of 68 and 20 ms (for methyl and phenyl respectively). These values can only be taken as completely independent if spin diffusion is not effective, which is presumably the case because MAS results in resolution in the ^1H spectrum. In the solid state overall molecular motion will be slow, but there may be fast reorientation of certain groups within a molecule.

In the $(PhF_2PNMe)_2$ case the two doublets for the axial and equatorial fluorines can be observed separately. For the proton T_1 similar values are obtained from the two fluorine resonances *via* ^1H inversion followed by CP, and an average time is appropriate. The error in the measured integrals and the similarity of the two plots (intensity *vs*. time) show that this is valid.

The F_3 compound, which exhibits fast Berry pseudo-rotation around phosphorus on the NMR timescale at room temperature, has a short proton (NPh) spin–lattice relaxation time (2.5 s) and a very short T_1^F of 0.3 s.

There is close similarity between the T_1^H values for the two fluorinated compounds containing both PPh and NMe groups. This implies the effect of the NMe protons dominates due to their fast internal rotation. Somewhat surprisingly, the T_1^F values for the difluoro case are significantly longer than that for $(Ph_2FPNMe)_2$. However, that for $(F_3PNMe)_2$ is very short. It can be seen that the relaxation times are not merely dependent on the number of fluorines in the molecule. All these measurements are at ambient probe temperature and therefore relate to mobility at *ca*. 26 °C.

Conclusion

The number of resonances observed in a solid-state NMR spectrum is related to the asymmetric unit of a structure. The spectra recorded for these compounds indicate that, despite being dimeric structures, only single ^{19}F, ^{31}P and ^{15}N environments are observed. Any multiplicity of lines can be explained by coupling or the loss of averaging of multiple fluorine sites. This is consistent with the reported crystal structure[6] of $(PhF_2PNMe)_2$. However, we do not resolve separate peaks for the two independent molecules in the crystal structure[7] of $(Ph_2FPNMe)_2$.

Rates of motion within the molecule are affected by both substituents on the phosphorus and nitrogen in the ring. In the case of $(PhF_2PNMe)_2$ pseudo-rotation is shown to be slow on the NMR timescale in the solid state since separate signals are seen for axial and equatorial fluorines. Motion, at the fast limit at ambient probe temperature, makes all three fluorine sites equivalent in the PF_3 compound. As motion is slowed by lowering the temperature, complex patterns are observed in the phosphorus spectrum because of coupling to non-equivalent fluorines (the fluorine situation is simpler as each fluorine is coupled to a single phosphorus and chemical shifts separate the individual environments as exchange is slowed). In this case only the sum of the coupling constants is measurable, as the separation of the outermost lines. Phosphorus–fluorine coupling has been removed in spectra of both nuclei by high-power heteronuclear decoupling and has confirmed that PF indirect coupling is the cause of the splitting.

Although linewidths are substantially larger than for solutions, the solid-state chemical shifts are in agreement with the previous solution-state experiments (to within less than 2 ppm). This is true of the averaged chemical shifts when there are separate peaks, *i.e.* in the slow exchange limit, for the solid state. Thus there appear to be no chemically significant intermolecular interactions in the solid compounds.

Valuable information can be obtained from anisotropies, as measured from spinning sideband manifolds or static spectra, in terms of the effective dipolar interaction. In general, D and ΔJ are not readily mathematically separable, but in cases where crystal structure information is available D can be determined, giving a route to the anisotropy in J (though not to high accuracy).

Experimental

All the diazadiphosphetidines were provided by Professor R. Schmutzler and H. Thönnessen, Braunschweig University. Since the samples are subject to possible decomposition if exposed to moist air, they were initially handled in a glove-box and sealed in small plastic inserts, which then fit tightly into the rotors used. Recrystallisation of $(Ph_2FPNMe)_2$ was attempted using toluene to remove observed impurities. Even though complete purification was not obtained, significant improvement was found, bringing NMR signals from impurities down to acceptably low intensity.

The spectrometers used in this work were Chemagnetics CMX200 and Varian Unity Plus 300. The majority of the study was done on the lower field spectrometer. Four probes have been used. The diameters of the rotors are: HX and HFX, 7.5; HXY, 5; HF, 4 mm. These allow almost any combination of observation, cross-polarisation and decoupling, with the use of appropriate filters. The only obvious limitation is the inability to decouple protons while observing fluorine with the HFX probe. This means that, when decoupling phosphorus from fluorine, ^{19}F spectra have to be acquired without proton decoupling. Recycle delays were initially determined by variable delay-time experiments and checked by measurement of T_1^H where appropriate. For cross-polarisation experiments (nitrogen, carbon, phosphorus and some fluorine spectra) optimum contact times were found by arraying this parameter and choosing that with the greatest signal intensity. Spin rates used were generally 4–6 kHz with the 7.5 mm probes, 8 kHz for the 5 mm probe and in the range 10–15 kHz for the 4 mm probe.

The frequencies of the individual nuclei on the two spectrometers are: Chemagnetics CMX200 ^{31}P, 81.0; ^{13}C, 50.3; ^{19}F, 188.3; ^1H 200.1; ^{15}N, 20.3 MHz; Varian Unity Plus 300 ^{15}N, 30.4 MHz (used for $(Ph_2FPNMe)_2$ only). Referencing was done by replacement, setting the chemical shift scales as follows using the compounds named: ^{31}P, $CaHPO_4$ set to 1.2 ppm (w.r.t. 85% H_3PO_4 at zero ppm); ^{19}F, C_6F_6 set to −166.4 ppm w.r.t. $CFCl_3$; ^{13}C, high-frequency peak of adamantane set to 38.4 ppm w.r.t. $(CH_3)_4Si$; and ^{15}N, nitrate peak of ammonium nitrate set to 5.1 ppm w.r.t. CH_3NO_2. For fluorine acquisition, with high-power proton decoupling, the Bloch–Siegert shift was corrected experimentally by obtaining reference spectra with the proton decoupling frequency applied.

In all cases, however, the standard MAS, direct or cross-polarisation sequences gave good ^{19}F NMR spectra with sufficient resolution to be able to use deconvolution to extract shift, intensity and linewidth parameters, so that CRAMPS (combined rotation and multiple pulse spectroscopy) operation was not necessary.

The temperatures have been calibrated using data obtained from the proton spectra of methanol on tetrakis(trimethylsilyl)-

silane.[38] The experimental spin-rate and temperature conditions were used to record the change in frequency separation of the two peaks, which is directly related to actual sample temperature. Thus calibration graphs were produced. In fast-spinning cases the calibrated temperature is significantly higher than the set temperature.

Spinning sideband analysis was done using an in-house program, ssb97,[33] based on the theory of Maricq and Waugh,[39] which includes the error analysis of Olivieri.[40] Between 5 and 11 peaks were fitted for the sideband manifolds analysed. The static bandshape simulation used a program RZX NMR analysis package with a visual interface 'd8'.[41]

Fluorine-19 spin–lattice relaxation times have been measured using the Torchia sequence,[36] *i.e. via* $^{1}H \longrightarrow {}^{19}F$ CP followed by a 90° ^{19}F pulse, a variable delay and a 90° ^{19}F read pulse. Proton decoupling was applied during acquisition but not during relaxation. In general, coupled spin systems will not yield single exponential plots for relaxation times. However, the present measurements generally showed reasonably single-exponential curves. Considering any random scatter in intensity measurements, the errors in the exponential fits do not indicate that the equations are inappropriate for these cases. For proton spin–lattice relaxation times the pulse sequence consists of a 180° pulse on the proton channel followed by a variable delay, then a 90° ^{1}H pulse and contact to observe ^{31}P NMR spectra. Measurements generally have statistical errors of ≈2–8%, with the larger values being for longer relaxation times, where the end of the decay is not observed due to, for instance, limits on spin-lock time.

In addition to the ^{19}F, ^{31}P and ^{15}N NMR spectra discussed in the text, ^{13}C CPMAS spectra of $(Ph_2FPNMe)_2$ and $(PhF_2PNMe)_2$ were measured using a variety of techniques and the results are reported in Table 1 for completeness. Thus dipolar dephasing has been employed to locate the signals from the methyl carbons and the *ipso* carbons of the phenyl groups. For such experiments contact times of 2 ms and recycle delays of 60 s were used. For $(PhF_2PNMe)_2$ the *ipso* carbon signal was found to be at δ_C 133, which was confirmed by $^{31}P \longrightarrow {}^{13}C$ CP, with high-power proton decoupling in a triple-resonance experiment. This experiment required a recycle delay of 360 s because of the long T_1 for ^{31}P, but a contact time of 5 ms was optimum. A variable amplitude (ramped) CP sequence[42,43] was found to give a more intense signal than simple CP in a given time for $^{31}P \longrightarrow {}^{13}C$ CP.

Acknowledgements

We are very grateful to Professor R. Schmutzler and H. Thönnessen, from Braunschweig University, Germany for synthesis of the diazadiphosphetidines. We thank Dr J. Evans (Durham University) for assistance with the X-ray powder diffraction. One of us (L. A. C.) thanks the EPSRC for a studentship and for access to the Durham-based research service in solid-state NMR (UDIRL). We acknowledge the receipt of research grant GR/L02906 from the U.K. Engineering and Physical Sciences Research Council in support of this work.

References

1 R. K. Harris, M. I. M. Wazeer, O. Schlak and R. Schmutzler, *J. Chem. Soc.*, *Dalton Trans.*, 1976, 17.
2 R. K. Harris, M. I. M. Wazeer, O. Schlak and R. Schmutzler, *J. Chem. Soc.*, *Dalton Trans.*, 1974, 1912.
3 O. Schlak, R. Schmutzler, R. K. Harris and M. Murray, *J. Chem. Soc.*, *Chem. Commun.*, 1973, 23.
4 O. Schlak, R. Schmutzler and I. K. Gregor, *Org. Mass Spectrom.*, 1974, **9**, 582.
5 A. Almenningen, B. Andersen and E. E. Astrup, *Acta Chem. Scand.*, 1969, **6**, 2179.
6 R. K. Harris, M. I. M. Wazeer, O. Schlak, R. Schmutzler and W. S. Sheldrick, *J. Chem. Soc.*, *Dalton Trans.*, 1977, 517.
7 P. G. Jones and R. Schmutzler, *Phosphorus Sulfur Silicon Relat. Elem.*, 1991, **56**, 173.
8 R. K. Harris, J. R. Woplin, R. E. Dunmur, M. Murray and R Schmutzler, *Ber. Bunsenges. Phys. Chem.*, 1972, **76**, 44.
9 R. K. Harris and C. M. Woodman, *Mol. Phys.*, 1966, **10**, 437.
10 R. Schmutzler and G. S. Reddy, *Inorg. Chem.*, 1965, **4**, 191.
11 R. Schmutzler, in *Halogen Chemistry*, ed. V. Gutmann, Academic Press, London, 1967, vol. 2, p. 31.
12 C. Shumann, H. Dreeskamp and O. Stelzer, *Chem. Commun.*, 1970, 619.
13 R. S. Berry, *J. Chem. Phys.*, 1960, **32**, 933.
14 R. K. Harris, M. I. M Wazeer, O. Schlak and R. Schmutzler, *Phosphorus Sulfur.*, 1981, **11**, 221.
15 D. P. Burum and W. K. Rhim, *J. Chem. Phys.*, 1979, **71**, 944.
16 U. Scheler and R. K. Harris, *Chem. Phys. Lett.*, 1996, **262**, 137.
17 S. F. Dec, C. E. Bronniman, R. A. Wind and G. E. Maciel, *J. Magn. Reson.*, 1989, **82**, 454.
18 S. A. Carss, U. Scheler, R. K. Harris, P. Holstein and R. A. Fletton, *Magn. Reson. Chem.*, 1996, **34**, 63.
19 R. K. Harris, S. A. Carss, R. D. Chambers, P. Holstein, A. P. Minoja and U. Scheler, *Bull. Magn. Reson. A*, 1995, **17**, 37.
20 S. A. Vierkötter, *J. Magn. Reson. A*, 1996, **118**, 84.
21 P. Holstein, U. Scheler and R. K. Harris, *Magn. Reson. Chem.*, 1997, **35**, 647.
22 A. Nordon, R. K. Harris, L. Yeo and K. D. M. Harris, *Chem. Commun.*, 1997, 2045.
23 R. K. Harris, K. J. Packer and A. M. Thayer, *J. Magn. Reson.*, 1985, **62**, 284.
24 U. Haubenreisser, U. Sternberg and A. R. Grimmer, *Mol. Phys.*, 1987, **60**, 151.
25 K. W. Zilm and D. M. Grant, *J. Am. Chem. Soc.*, 1981, **103**, 2913.
26 J. C. Cherryman and R. K. Harris, *J. Magn. Reson.*, 1997, **128**, 21.
27 J. C. Cherryman, R. K. Harris, M. G. Davidson and R. D. Price, *J. Brazilian Chem. Soc.*, in the press.
28 R. Schmutzler, *J. Chem. Soc.*, *Dalton Trans.*, 1973, 2687.
29 R. K. Harris and M. I. M. Wazeer, *Ber. Bunsenges. Phys. Chem.*, 1979, **83**, 697.
30 R. K. Harris, M. Lewellyn, M. I. M. Wazeer, J. R. Woplin, R. E. Dunmur, M. J. C. Hewson and R. Schmutzler, *J. Chem. Soc.*, *Dalton Trans.*, 1975, 61.
31 S. Hayashi and K. Hayamizu, *Chem. Phys. Lett.*, 1989, **161**, 158; G. Wu and R. E. Wasylishen, *J. Chem. Phys.*, 1993, **98**, 6138.
32 R Schmutzler, *Chem. Commun.*, 1965, 19.
33 J. R. Ascenso, L. H. Merwin, H.-P. Bai and J. C. Cherryman, unpublished work.
34 A. R. Grimmer and U. Haubenreisser, *J. Fluorine Chem.*, 1985, **29**, 244.
35 J. Sandstrom, *Dynamic NMR spectroscopy*, Academic Press, New York, 1982.
36 D. A. Torchia, *J. Magn. Reson.*, 1978, **30**, 613.
37 S. Ando, R. K. Harris and S. A. Reinsberg, *J. Magn. Reson.*, 1999, **141**, 91.
38 A. E. Aliev and K. D. M. Harris, *Magn. Reson. Chem.*, 1994, **32**, 366.
39 M. M. Maricq and J. S. Waugh, *J. Chem. Phys.*, 1979, **70**, 3300.
40 A. C. Olivieri, *J. Magn. Reson. A*, 1996, **123**, 207.
41 E. Hughes, University of South Carolina, 1995.
42 O. B. Peerson, X. Wu, I. Kustanovich and S. O. Smith, *J. Magn. Reson. A*, 1994, **106**, 127.
43 G. Metz, X. Wu and S. O. Smith, *J. Magn. Reson. A*, 1994, **110**, 209.

Paper 9/07142C